Electronic Supplementary Material (ESI) for Journal of Materials Chemistry A.

Supporting information

New Strategies to Improve Two-Electron Oxygen Reduction Reaction Selectivity of Polypyrrole-based Catalysts

Miaohui Wang, Jianhua Wang, Peipei Huang*, Haiping Lin*, Qing Li*

School of Physics and Information Technology, Shaanxi Normal University, No. 620, West Chang'an Avenue, Chang'an District, Xi'an, 710119, Shaanxi, PR China

E-mail: liqing@snnu.edu.cn; hplin@snnu.edu.cn; huangpeipei@snnu.edu.cn

1. Rotating Ring Disk Electrode (RRDE) collection efficiency.

Linear sweep voltammetry measurements were carried out in 0.01M $K_3Fe(CN)_6$ and 0.1 M KCl with a rotation rate between 400 and 1600 rpm, as shown in Fig. S1(a). The ring electrode potential is set to 1.55 V (*vs*. RHE). The ring current and disk current at 0.9 V (*vs*. RHE) were acquired to make the linear fitting. The collection efficiency is 0.45 from the linear fitting (Fig. S1(b)), which is close to the calculated value of 0.43[1].

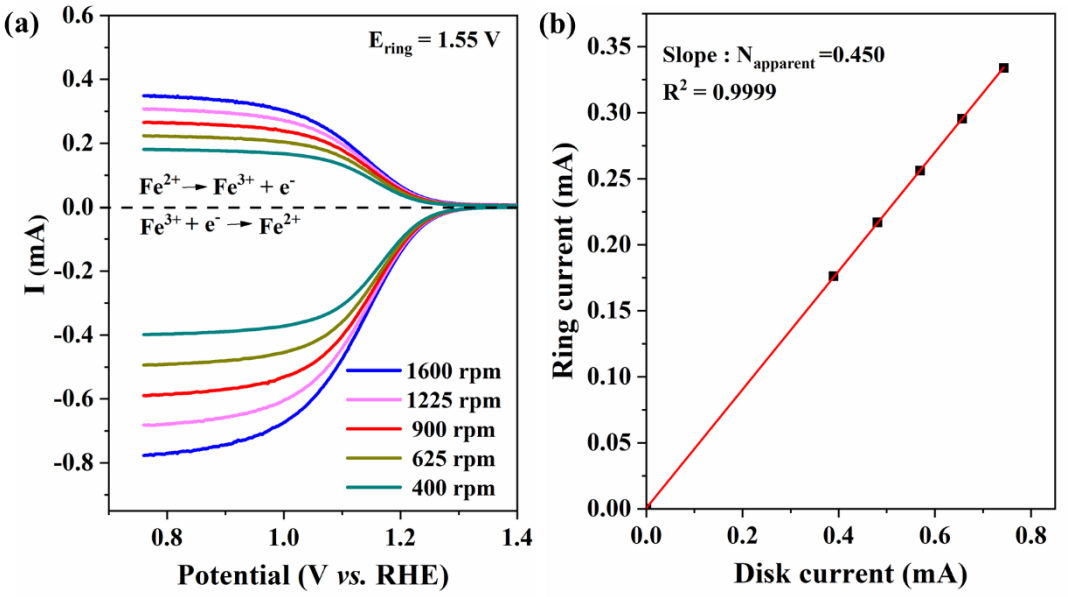

Fig. S1 RRDE collection efficiency calibration. (a) Linear sweep voltammetry on bare glassy carbon electrolyte with 0.01M $K_3Fe(CN)_6$ and 0.1 M KCl. Sweep rates: 50 mV/s. (b) Linear fitting of the limiting diffusion current on disk and ring electrodes at different rotational speed.

2. Scanning electron microscopy (SEM) images of the samples.

As shown in Fig. 2, all the samples exhibit irregular sphere-like morphology and sphere-like morphology remain unchanged during the calcining procedure and the introducing of phytic acid before polymerization.

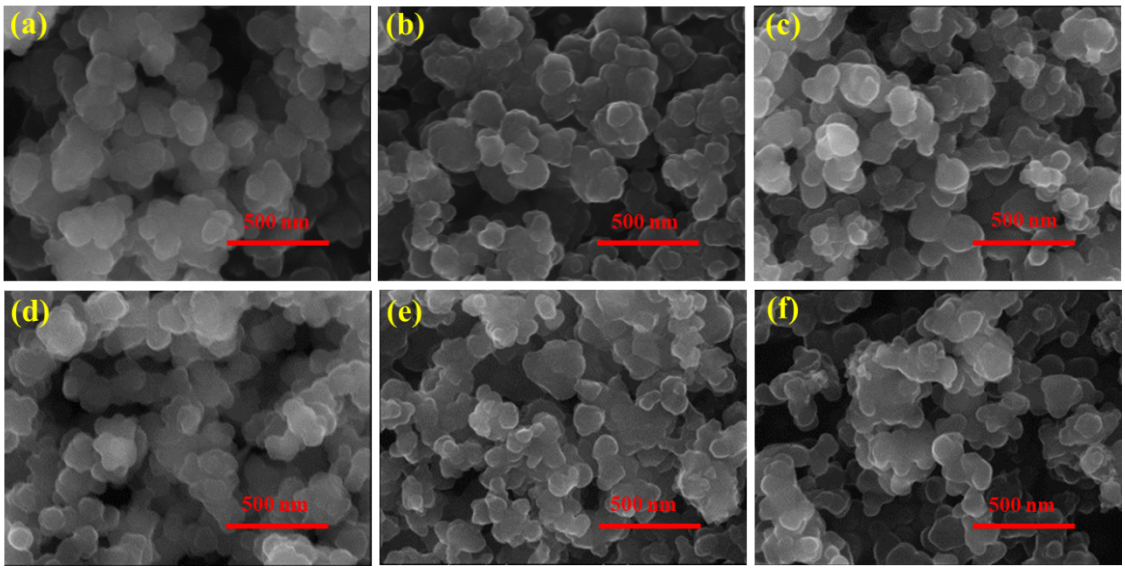

Fig. S2 SEM images of (a) NC, (b) NC-400, (c) NC-700, (d) NPC, (e) NPC-400 and (f) NPC-700.

3. X-ray photoelectron spectroscopy (XPS) spectra of NC, NPC and their derivates.

XPS wide-scan survey spectra of NC, NPC and their derivatives are shown in Fig. S3(a), in which the presence of elements can be confirmed (C1s at 284.8 eV, N1s at 400.6 eV, P2s at 191.2 eV, P2p at 133.8 eV and O1s at 532.1 eV) in the samples[2], which agree well with the EDS results (Fig. 1(c)). High resolution spectra (Fig. S3(b)) of C1s in all the samples were deconvoluted with peaks around 284.8, 285.8, 286.7 and 288.9 eV, which are ascribed to C=C/C-C, C-P, C-O/C-N and C=O groups[3], respectively. High-resolution P2p spectra (Fig. S3(c)) of NPC and its derivatives show three characteristic peaks at 132.5 eV, 133.6 eV and 134.2 eV, which can be attributed to P-C, P-O and P=O species[3-5], respectively.

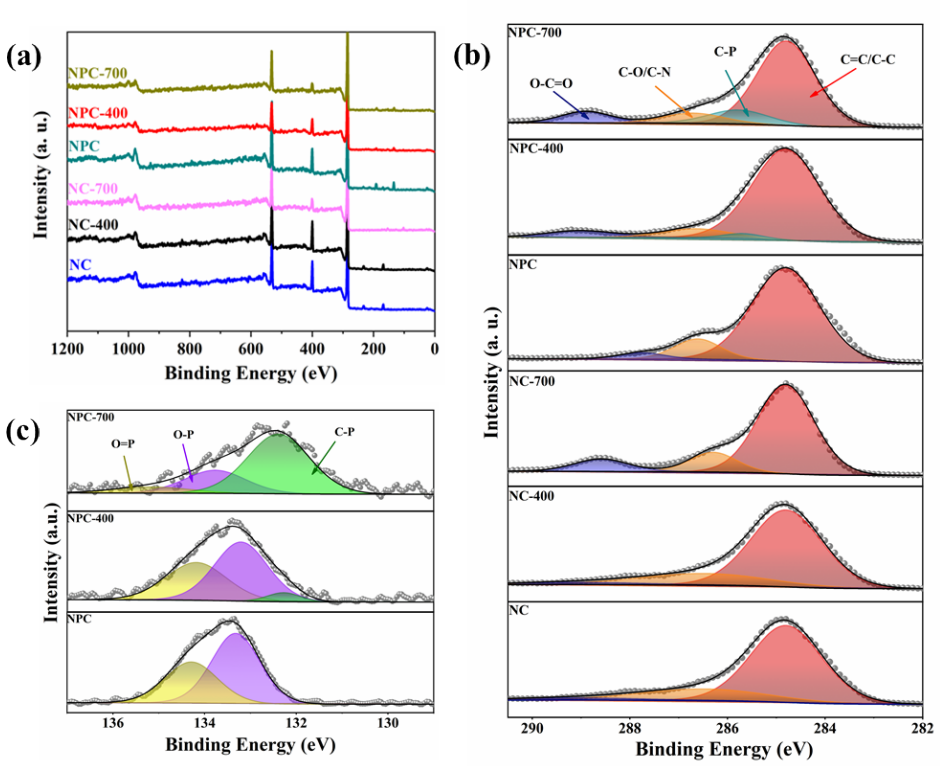

Fig. S3 XPS wide-scan spectra of (a) NC, NPC and their derivatives and high resolution spectra of (b) C1s in all the above samples and (c) P2p in NPC and its derivates.

4. Selectivities of H_2O_2 generation over NC-600, NC-700, NPC-600 and NPC-700.

Figure S4 gives the catalytic selectivities toward H_2O_2 generation over the calcined samples. Due to the significant escape of nitrogen and phosphorus atoms after high temperature calcination (see Table S1 for details), the catalytic selectivities toward H_2O_2 generation decreased dramatically.

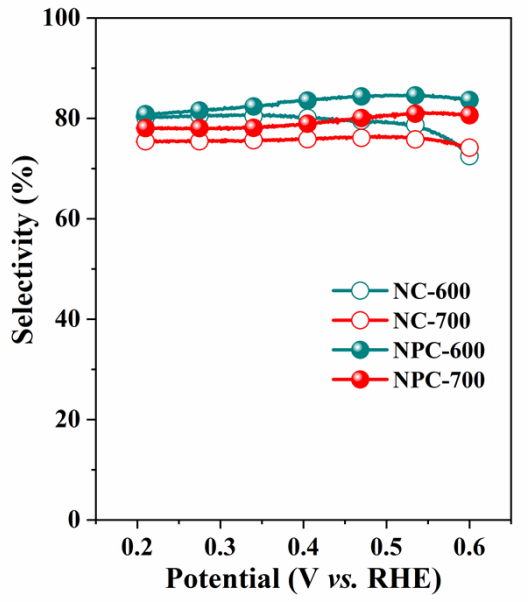

Fig. S4 The catalytic selectivities of H_2O_2 generation over NC-600, NC-700, NPC-600 and NPC-700.

5. Electrochemical impedance spectra (EIS)

Figure S5 gives the electrochemical impedance spectra (EIS) from 1 M Hz to 100 Hz at the potential being 0.1 V (*vs*. RHE). The intersection of the semicircle with the horizontal axis represents the charge transfer resistance. NPC-400 exhibits smallest diameter of the semicircles in Nyquist plots, indicating NPC-400 has smallest charge transfer resistance.

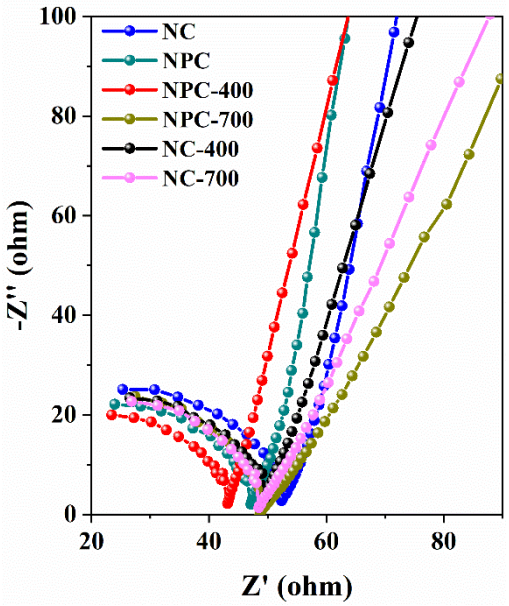

Fig. S5 The electrochemical impedance spectra of all samples.

6. Stability of NPC-400

As shown in Fig. S6, the H_2O_2 selectivity of NPC-400 almost remains unchanged after four months, suggesting this catalyst has excellent stability.

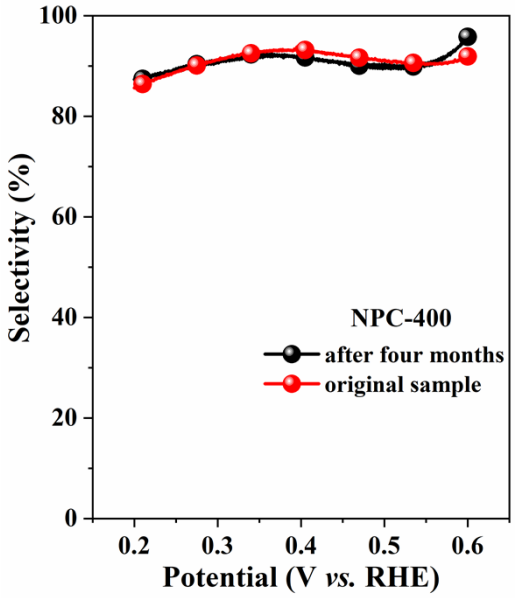

Fig. S6 Electrocatalytic performances of NPC-400 before (in red) and after (in black) four months.

7. H_2O_2 selectivity of different catalysts

Several different catalysts were tested to clarify the saturation of -N^+- species leads to the enhancement of H_2O_2 selectivity. 400 μL pyrrole and 1 mmol phytic acid were dispersed in 2 mL mixed solvent ($V_{ethanol}$:V_{water}=1:1) and 684 mg ammonium persulfate was dissolved in another 2 mL of the same mixed solvent. After cooling the above two solutions in an ice bath, polymerization reaction took place by mixing them together. The black hydrogel was aged for 24 h and then rinsed with water and ethanol, respectively. The catalyst (referred to as NPC) was obtained by freeze-drying. The synthesis procedures of NCP and NCC were basically the same as that of NPC except that 1 mmol phytic acid was replaced by phosphorous acid and glucose, respectively. The obtained catalysts of NC, CB (carbon black), NPC, NCC, and NCP were solid powder. The working electrode was prepared with the following method: 4 mg powder catalyst was dispersed in 1 mL mixed solution containing 700 μL isopropanol, 200 μL deionized water and 100 μL Nafion solution (5 wt%). The homogeneous ink was acquired after ultrasonication for 30 min. 5.83 μL of the above ink was coated onto the rotating ring disk electrode. When PA (phytic acid) was tested ORR performance, there was a little difference during the preparation of working electrode, 4 mg powder catalyst was replaced by 1mmol phytic acid.

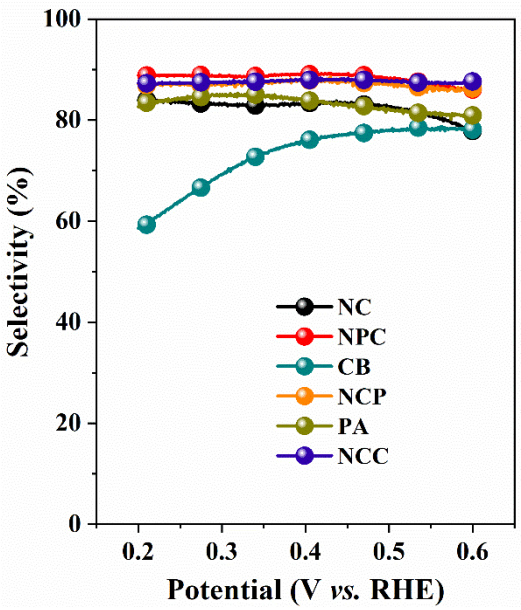

Fig. S7 H_2O_2 selectivities over different catalysts. CB represents pure carbon black sample, and PA represents pure phytic acid. NCP represents the samples, in which phosphorus acid was introduced before polymerization. NCC represents the samples, in which glucose were introduced before polymerization.

8. Electrochemically active surface areas *(ECSA)* of all catalysts

The electrochemically active surface areas are measured by the electrochemical double-layer capacitance method, in order to obtain the effective catalytic activity of the catalysts. The double layer capacitance is obtained by scanning the cyclic voltammetry curves at different sweep speeds (20, 40, 60, 80 and 100 mV/s, respectively), in the potential region of non-Faradaic reaction (1.01 V - 1.11 V *vs*. RHE).

The relation between the electrochemical surface areas and the capacitance is shown as follows[6-9]:

$$ECSA = C_{DL}/C_S$$

The relation between the charging current, the scanning speed and the capacitance of the double layer is given by:

$$i_c = vC_{DL}$$

where *Cs* is the specific capacitance of the catalyst or the capacitance of an atomically smooth planar surface of the material per unit area under identical electrolyte conditions[10]. C_{DL} is the capacitance of the double layer. Therefore, the *ECSA* is positive correlated with the capacitance of the double layer. *v* is the scanning speed set in cyclic voltammetry test and *ic* is the current density at different scanning speeds. The C_{DL} can be obtained by fitting the current values at different scanning speeds.

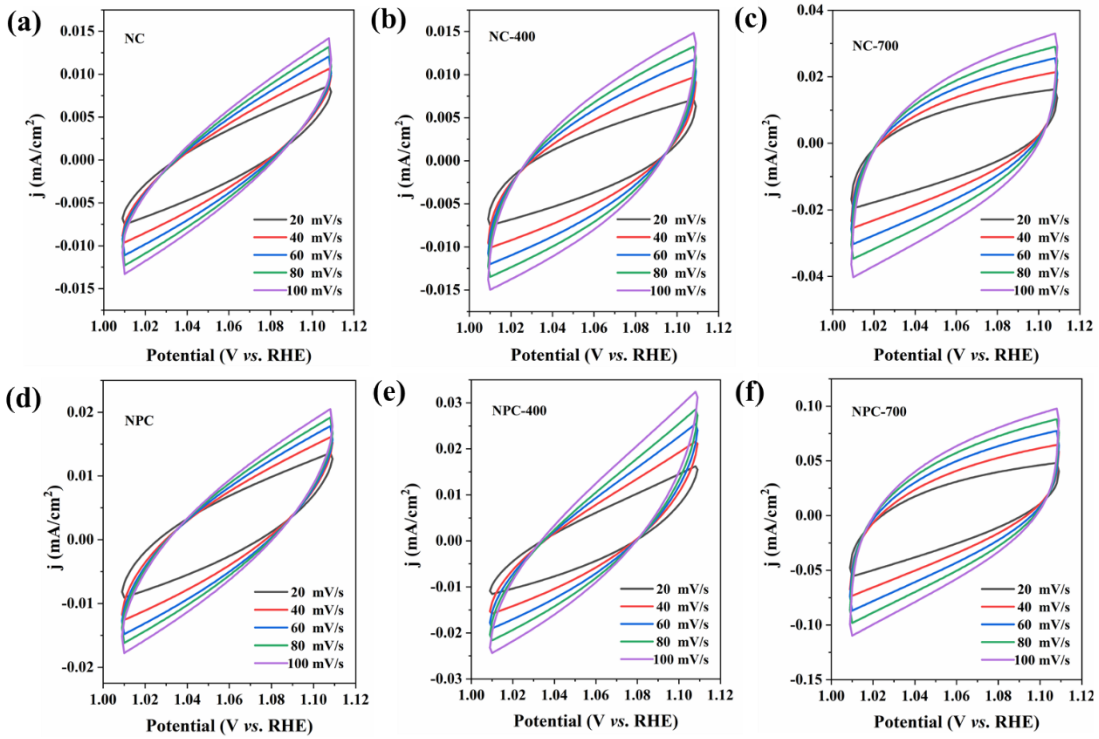

Fig. S8 Cyclic voltammetry curves of (a) NC, (b) NC-400, (c) NC-700, (d) NPC, (e) NPC-400 and (f) NPC-700 in non-Faradaic potential region (1.01 V - 1.11 V *vs*. RHE) with different sweep rates ranging from 20 to 100 mV/s.

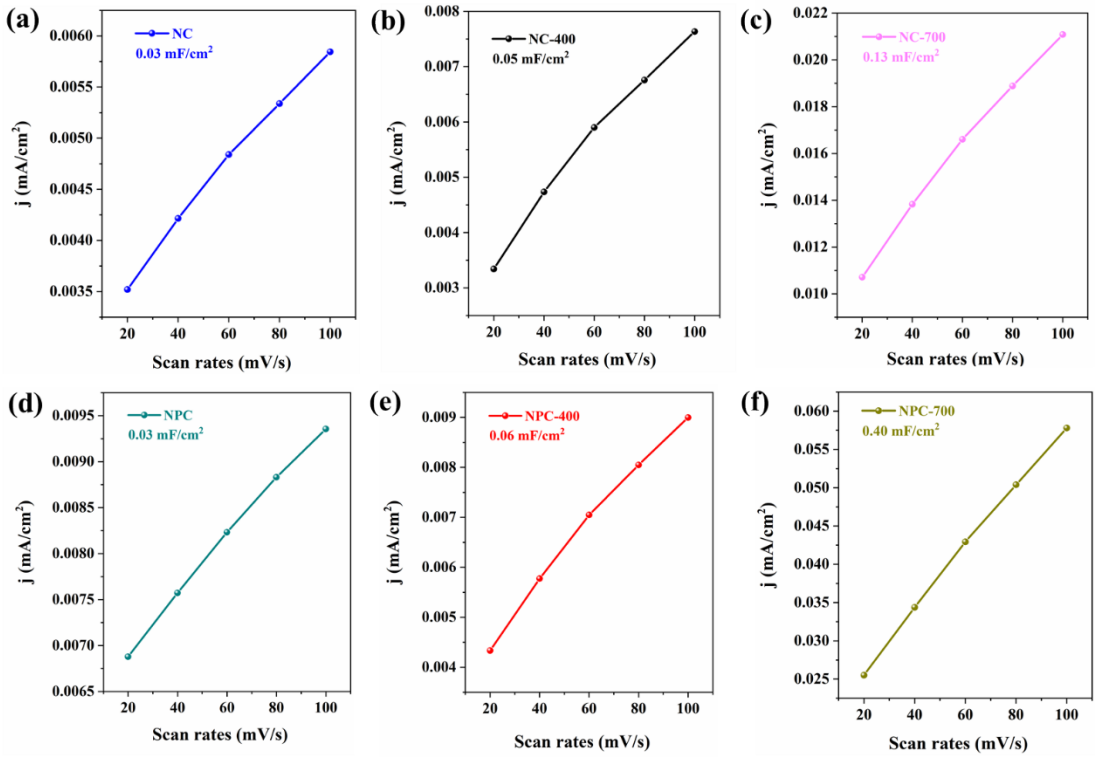

Fig. S9 Linear fitting of capacitive currents of (a) NC, (b) NC-400, (c) NC-700, (d) NPC, (e) NPC-400 and (f) NPC-700. Charging currents measured at 1.06 V *vs*. RHE were acquired to make the linear fitting.

With the increase of the calcination temperature, the ECSA of both NC and NPC increase gradually. NPC-400 (0.06 mF/cm^2) and NC-400 (0.05 mF/cm^2) do not have the highest ECSA but they show much better selectivities to H_2O_2 generation than the other samples. According to the XPS measurements (Fig. 3), the content of nitrogen significantly decreased significantly when the calcination temperature reaches 700 °C. Despite that the value of ECSA of NC-700 (0.13 mF/cm^2) and NPC-700 (0.40 mF/cm^2) are higher than that of the other samples, their selectivity to H_2O_2 production exhibit obviously lower than the other samples. These results strongly demonstrate that the porous structure and the specific surface area do not play considerable influence on the H_2O_2 formation. However, it is the α carbon atoms of pyrrolic-N in polypyrrole-based catalysts that are the active sites for the selective H_2O_2 production. Combining the characterizations, control experiments and DFT calculations, decreasing the formation of deprotonated nitrogen species in polypyrrole-based catalysts by hydrogen-bonding interaction during the polymerization of pyrrole or transforming -N^+- species to be C-N bonds by calcination are feasible strategies to achieve higher selectivity to H_2O_2 generation.

9. Repeated experiments with all catalysts

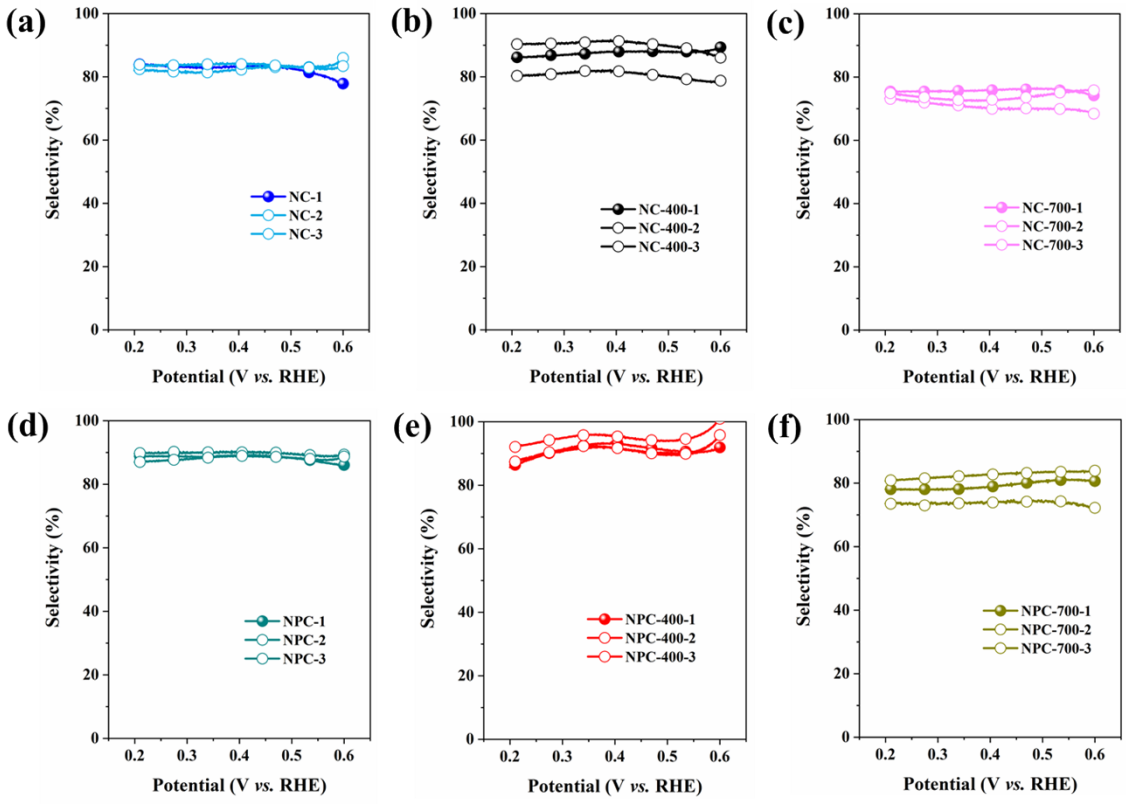

Fig. S10 The reproducibility of the selectivity measurements. The solid dots are the same as the data shown in Fig. 5a

10. Elemental contents of all samples

From the XPS measurement results, we obtained the respective weight of the elements in NC, NC-400, NC-700, NPC, NPC-400 and NPC-700, respectively, as shown in Table S1.

Table S1 Elemental contents of C, N, O, P and S of all the samples.

Sample	Chemical composition (at %)				
	C	N	O	P	S
NC	68.85	13.26	15.85	--	2.04
NC-400	75.18	8.17	16.23	--	0.42
NC-700	77.79	6.98	14.86	--	0.41
NPC	61.96	12.3	20.54	4.07	1.12
NPC-400	76.05	9.1	12.31	2.18	0.36
NPC-700	77.96	5.67	14.39	1.61	0.37

References

1. K. Jiang, S. Back, A. J. Akey, C. Xia, Y. Hu, W. Liang, D. Schaak, E. Stavitski, J. K. Norskov, S. Siahrostami and H. Wang, *Nat Commun*, 2019, **10**, 3997.
2. K. Yuan, D. Lutzenkirchen-Hecht, L. Li, L. Shuai, Y. Li, R. Cao, M. Qiu, X. Zhuang, M. K. H. Leung, Y. Chen and U. Scherf, *J Am Chem Soc*, 2020, **142**, 2404-2412.
3. M. Ben Ali, F. Wang, R. Boukherroub, W. Lei and M. Xia, *J Colloid Interface Sci*, 2019, **553**, 688-698.
4. Z. Yang, Y. Gao, Z. Zhao, Y. Wang, Y. Wu and X. Wang, *Journal of Power Sources*, 2020, **474**.
5. J. Deng, S. Chen, Q. Zhou, Y. Nie, J. Li, R. Wu, Q. Wang and Z. Wei, *Journal of Power Sources*, 2020, **451**.
6. Y. Zhou, Y. Sun, H. Wang, C. Zhu, J. Gao, D. Wu, H. Huang, Y. Liu and Z. Kang, *Inorganic Chemistry Frontiers*, 2018, **5**, 2985-2991.
7. Y. Zhou, Y. Sun, C. Zhu, Y. Liu, X. Dai, J. Zhong, Q. Chen, H. Tian, R. Zhou and Z. Kang, *Journal of Materials Chemistry A*, 2018, **6**, 8955-8961.
8. G. Gryglewicz, J. Machnikowski, E. Lorenc-Grabowska, G. Lota and E. Frackowiak, *Electrochimica Acta*, 2005, **50**, 1197-1206.
9. J. D. Benck, Z. Chen, L. Y. Kuritzky, A. J. Forman and T. F. Jaramillo, *ACS Catalysis*, 2012, **2**, 1916-1923.
10. T. A. Centeno and F. Stoeckli, *Journal of Power Sources*, 2006, **154**, 314-320.